Highlights

A Hybrid Domain Overlapping Method for Coupling System Thermal Hydraulics and CFD Codes

Aaron Huxford,Victor Coppo Leite,Elia Merzari,Ling Zou,Victor Petrov,Annalisa Manera

- A hybrid domain overlapping coupling method is presented.
- Numerical stability is compared against a domain decomposition method using two loop configurations.
- Proposed method found to exhibit more favorable stability behavior.
- Proposed method is validated against experimental data considering three-dimensional scalar mixing.

A Hybrid Domain Overlapping Method for Coupling System Thermal Hydraulics and CFD Codes

Aaron Huxford[a,*], Victor Coppo Leite[b], Elia Merzari[b], Ling Zou[c], Victor Petrov[a,d,e] and Annalisa Manera[a,d,e]

[a]Department of Nuclear Engineering and Radiological Sciences, University of Michigan, Ann Arbor, MI, USA
[b]Department of Nuclear Engineering, Penn State University, State College, PA, USA
[c]Nuclear Science and Engineering Division, Argonne National Laboratory, Lemont, IL, USA
[d]ETH Zurich, Department of Mechanical and Process Engineering, Zurich, Switzerland
[e]Laboratory for Reactor Physics and Thermal-Hydraulics, Paul Scherrer Institut, Villigen, Switzerland

ARTICLE INFO

Keywords:
Coupling
Overlapping
STH
SAM
CFD
NekRS

ABSTRACT

A hybrid multiscale coupling methodology based on a domain overlapping approach has been developed for coupling System Thermal Hydraulics (STH) and Computational Fluid Dynamics (CFD) codes. The method has been implemented between the modern STH code SAM and the CFD code NekRS, using the coupling tool Cardinal. The coupling aims to extend the STH code's applicability to scenarios where local momentum and energy transfers are important yet difficult for STH codes to capture, such as three-dimensional mixing.

Two coupling strategies are implemented and compared: a hybrid domain overlapping method and the conventional domain decomposition method. The strategies are applied to two closed-loop applications, and the present method showed superior stability behavior when compared to the domain decomposition method. Then, the present coupling method is validated against experimental data from a double T-junction experiment. The present STH/CFD coupling shows improved agreement with experimental data when compared to STH standalone simulations.

1. Introduction

One important problem in nuclear reactor safety analysis is how to compute the evolution of accident scenarios for accurately estimating reactor safety margins. Currently, government regulators accept results from System Thermal Hydraulics (STH) codes if the physical conditions of application are within the code's range of validation. STH codes utilize a simplified, 1D (one-dimensional) description of the nuclear power plant, and to augment the simplified models, they rely on a large number of closure correlations typically based on experimental data. When 3D (three-dimensional) flow effects play an important role in the system, the STH code's simplifying 1D assumptions face many challenges and can even become invalid. In current and next-generation nuclear reactor systems, components such as the reactor pressure vessel, containment compartments and pools contain 3D flow and mixing effects that can play an important role in the evolution of accident scenarios. For example, during a loss of forced-cooling accident, a Modular High Temperature Gas-cooled Reactor's upper plenum can contain 3D mixing and thermal striping due to reversed flow within the reactor's core (Huning et al. (2021)). During a similar protected loss of forced-cooling accident, a pool-type Sodium-cooled Fast Reactor's sodium pool contains heat and mass transfer that produces thermal stratification, which is inherently a three-dimensional process (Wu et al. (2020)). Computational Fluid Dynamics (CFD) codes can provide more-accurate predictions of complex 3D flow phenomena than STH codes. Over recent years, CFD codes have been increasingly applied to the simulation of single-phase flow in complex nuclear reactor systems due to the increased maturity of CFD models and increased availability of computational resources (Smith et al. (2008)). However, modeling an entire reactor system with CFD remains prohibitively computationally expensive. As a result, the coupling of CFD with STH codes to take full advantage of CFD's modeling accuracy and STH's computational efficiency is an important undertaking.

1.1. Previous STH/CFD Coupling

In recent years, there have been several efforts in coupling STH/CFD codes using various STH and CFD codes, coupling methods, and computational domain decomposition methods. For a full overview of recent work in the field, the authors direct readers to Long et al. (2021) and Pucciarelli et al. (2021). STH/CFD coupling methods are placed into two major categories: explicit or semi-implicit. In explicit coupling, the codes advance a coupled time step in sequence, and each code solves the time step only once. In semi-implicit coupling, each code solves the time step multiple times until the coupled step reaches a problem-specific convergence criteria. STH/CFD coupling's computational domain decomposition methods are placed into two major categories as well: domain decomposition and domain overlapping. The domain decomposition method splits the modeled system into separate STH and CFD domains, and data transfers occur at the boundaries of each code's domain. For the domain overlapping method, the STH code models the entire domain, including a component that overlaps with

*Corresponding author
ahuxford@umich.edu (A. Huxford)

the CFD-modeled domain. Here, data transfers occur at the boundaries of the CFD domain, and the overlapping STH component's internal nodes receive a CFD-informed model coefficient in the form of a friction factor or form loss coefficient.

The majority of previous STH/CFD coupling implementations utilize an explicit coupling approach along with the domain decomposition method (Aumiller et al. (2001); Schultz and Weaver (2003); Anderson (2006); Papukchiev et al. (2009); Liu et al. (2010); Yan et al. (2011); Bavière et al. (2014); Cho et al. (2014); Li et al. (2014); Martelli et al. (2014); Watanabe et al. (2014); Tangtao et al. (2017)). In an effort to improve the domain decomposition method's stability at the boundaries of the STH and CFD domains, authors have pursued the semi-implicit coupling method (Bertolotto et al. (2009); Martelli et al. (2014); Theodoridis et al. (2014); Toti et al. (2017)). Bertolotto et al. (2009) utilized explicit and semi-implicit coupling methods with the domain decomposition method, and the semi-implicit coupling method showed superior stability behavior compared to explicit coupling. The semi-implicit method provides improved numerical stability but requires the recalculation of coupled time steps, which can be too computationally costly for the CFD code. A fully-implicit coupling method has also been pursued by Park et al. (2013), but such a coupling requires a large amount of user intervention into the STH and CFD source code and as well as underlying knowledge of the internal solvers.

To improve numerical stability of the explicit coupling method without requiring the CFD code to rerun time steps, authors have pursued domain overlapping methods where the STH domain contains a component overlapping with the CFD domain. Grunloh and Manera (2016) performed explicit coupling with domain decomposition and domain overlapping method where the authors informed the overlapping STH component using a CFD-informed friction factor coming from the CFD solution. The domain overlapping method showed superior stability compared to the domain decomposition method without the additional computational requirements required for semi-implicit coupling. However, the authors did not specify energy coupling or additional passive scalar coupling.

1.2. Present STH/CFD Coupling

In the paper, the authors present a hybrid domain overlapping coupling method that applies and extends Grunloh and Manera (2016)'s domain overlapping method to energy and passive scalar coupling. This addition enables the coupling method for the analysis of pool-type reactor systems where 3D flow is governed by buoyancy effects via spatial temperature gradients. Here, the coupling is applied between the advanced reactor STH code SAM (Hu et al. (2021)) and the GPU-oriented CFD code NekRS (Fischer et al. (2021)) using the coupling tool Cardinal (Merzari et al. (2021); Novak et al. (2022)) to facilitate code execution and in-memory data transfers. The traditional domain decomposition method is also employed for comparison purposes.

2. Software Used

2.1. STH code: SAM

SAM (System Analysis Module) is a modern STH code aimed at advanced non-LWR safety analysis and is under active development at Argonne National Laboratory. SAM aims to provide fast-running, whole-plant transient analyses capability with improved-fidelity for Sodium-cooled Fast Reactors, Lead-cooled Fast Reactors, and Molten Salt Reactors. SAM utilizes the open-source, NQA-1 compliant, object-oriented application framework MOOSE (Permann et al. (2020)) with its underlying meshing and finite-element library libMesh (Kirk et al. (2006)), and linear and nonlinear solvers PETSc (Balay et al. (2022)).

2.2. CFD code: NekRS

NekRS is an open-source, GPU-oriented CFD code based on the high-order spectral element method and includes an interface to its predecessor Nek5000. NekRS is under active development at Argonne National Laboratory. State of-the-art multilevel preconditioners, efficient high-order time-splitting methods, and runtime-adaptive communication strategies are built on a fast OCCA-based kernel library, libParanumal (Chalmers et al. (2022)), to provide scalability and portability across the spectrum of current and future high-performance computing platforms. NekRS is suited to model a wide range of spatial scales from Direct Numerical Simulations and Large Eddy Simulations to Reynolds-Averaged Navier Stokes (RANS). As an example of NekRS's applicability within the nuclear energy research community, Fischer et al. (2021) used NekRS to perform full-core Large Eddy Simulations of a pebble bed reactor with more than 350,000 pebbles. Also, Merzari et al. (2020) used NekRS to perform full-core Small Modular Reactor RANS simulations, showing NekRS's range of fidelity.

2.3. Coupling tool: Cardinal

Cardinal is an open-source wrapping of NekRS within the MOOSE framework (Permann et al. (2020)) and is under active development at Argonne National Laboratory. Cardinal can couple NekRS to other MOOSE-native or MOOSE-wrapped applications. One clear advantage of using the MOOSE framework for coupling is MOOSE's MultiApp system, (Gaston et al. (2015)) which facilitates code execution and data transfer timing. Cardinal uses a generic data transfer implementation that allows NekRS to be coupled to any MOOSE application, enabling a broad set of multiphysics and multiscale capabilities. Example uses of Cardinal include the following: Merzari et al. (2021) performed coupled Monte Carlo, thermal fluids and fuel performance simulations in pebble bed reactors; Novak et al. (2021) performed coupled conjugate heat transfer simulations for bypass flow modeling in pebble bed reactors; Novak et al. (2022a) performed coupled Monte Carlo and thermal hydraulics simulations of a prismatic gas reactor fuel assembly; and Novak et al. (2022b) performed coupled Monte Carlo transport and conjugate heat transfer simulations for wire-wrapped fuel bundles.

3. Coupling Methodology and Equations

The present work utilizes an explicit coupling implementation with both domain decomposition and domain overlapping methods to couple mass, momentum, energy, and passive scalar equations of single-phase incompressible flows (Huxford et al. (2022)). An explicit coupling method is utilized because it requires less computational resources than the semi-implicit coupling method, as well as far less user intervention. Diagrams of the domain methods are shown in Fig. 1, where $\boldsymbol{U}$ is velocity, $\boldsymbol{P}$ is pressure, $\boldsymbol{T}$ is temperature and f_{CFD} is a CFD-informed friction factor. The main difference between methods is that the domain overlapping method allows the STH code to model the entire domain, including the CFD-modeled portion. The CFD domain's solution is used to pass a CFD-informed friction factor to the overlapping STH component, which is expanded on in Section 3.1.

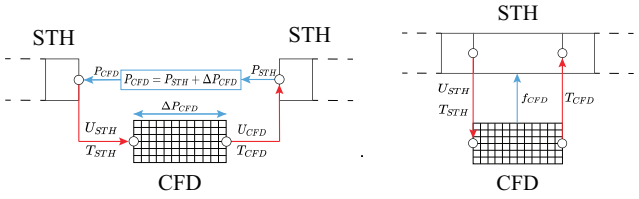

Figure 1: Coupling schematics for the domain decomposition (left) and hybrid domain overlapping (right) methods.

The domain overlapping method proposed by Grunloh and Manera (2016) was extended to coupling of the energy equation and passive scalar equations utilizing a domain decomposition-like approach. Unlike the strong coupling between velocity and pressure fields, temperature and passive scalars are less-coupled in space, such that a domain decomposition-like coupling is sufficient. That is, the present hybrid domain overlapping coupling method uses an overlapping methodology for momentum coupling and a domain decomposition methodology for energy and passive scalar coupling.

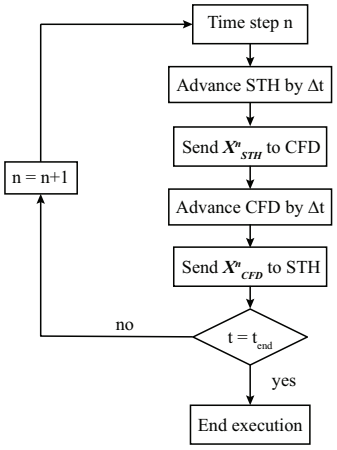

Figure 2: Explicit coupling scheme implemented.

The explicit coupling scheme implemented is shown in Fig. 2. The terms X^n_{STH} and X^n_{CFD} reflect data coming from the STH code and CFD code, respectively. Their description depends on the domain method, decomposition or overlapping, and are written in Table 1. Data coming from the CFD code are surface-averaged quantities over their corresponding boundary surface. For passive scalar coupling, additional scalars are transferred using the same method as temperatures T^n_{STH} and T^n_{CFD}.

Table 1
Data transfers for each coupling method.

Coupled Term	Coupling Method	
	Decomposition	Overlapping
X^n_{STH}	U^n_{STH}, T^n_{STH}	U^n_{STH}, T^n_{STH}
X^n_{CFD}	$U^n_{CFD}, P^n_{CFD}, T^n_{CFD}$	f^n_{CFD}, T^n_{CFD}

3.1. CFD-informed Friction Factor

Care needs to be taken when implementing the domain overlapping's f_{CFD} because the STH code may utilize either the Fanning or Darcy friction factor, which differ by a factor of four. To derive f_{CFD}, the authors follow the same procedure as Grunloh and Manera (2016). First, the CFD, NekRS momentum conservation equation and the equivalent STH, SAM 1D equation are outlined in Eq. (1) and Eq. (2), respectively. These equations are also followed by the solenoidal condition $\nabla \cdot \mathbf{u} = 0$ stemming from incompressible mass conservation.

$$\frac{\partial \mathbf{u}}{\partial t} + \mathbf{u} \cdot \nabla \mathbf{u} = -\frac{1}{\rho} \nabla P + \nabla \cdot \boldsymbol{\tau} - \mathbf{g} \tag{1}$$

$$\frac{\partial u}{\partial t} + u \frac{\partial u}{\partial x} = -\frac{1}{\rho} \frac{\partial P}{\partial x} - \frac{f}{D_e} \frac{u|u|}{2} - g \tag{2}$$

The domain overlapping coupling method uses a CFD-informed friction factor to ensure that given the same inlet velocity, the pressure gradient in SAM's overlapping component matches the NekRS solution. In order for the pressure gradients in Eq. (1) and Eq. (2) to match, the sum of SAM's convection, friction, and gravity terms should match the sum of NekRS's convection, viscous, Reynolds-stress, and gravity terms. To do so, SAM's convection and gravity terms in Eq. (2) are first removed to allow NekRS to model these effects. Then, SAM's friction term is equated to NekRS's inertial (including gravity) and friction terms, and the friction factor is solved for as the following CFD-informed friction factor:

$$f_{CFD} = -\frac{2 D_e}{\rho u |u|} \left[\nabla P + \rho \frac{\partial \mathbf{u}}{\partial t} \right]_{CFD}, \tag{3}$$

where $[\cdots]_{CFD}$ contains information from the NekRS CFD solution. The friction-factor in Eq. (3) depends on SAM's velocity u and is thus implemented as an implicit term within SAM's internal solver. Also, the overlapped portion of SAM solves a modified version of the momentum equation since NekRS is already modeling the convective and gravitational terms. This is especially important when buoyancy effects are present, such as during coupled modeling of natural circulation loops.

To use f_{CFD} from Eq. (3), a single value is computed for the entire overlapped STH component. The bracketed term with 3D CFD information is derived as a volume-averaged quantity. First, the 3D CFD data is dotted into a 1D flow direction, which is labeled by the flow path vector field $\hat{\mathbf{n}}_{fp}$. Then it is volume averaged using $\langle\cdot\rangle = \frac{1}{V}\iiint_V(\cdot)dV$. Doing so for the pressure gradient and inertial term in Eq. (3), the full form of f_{CFD} becomes:

$$f_{CFD} = \frac{2D_e}{\rho u|u|}\left[\frac{\Delta P^n_{CFD}}{L} - \frac{\rho}{\Delta t}\left(\frac{1}{V}\iiint(\mathbf{u}^{n+1}\cdot\hat{\mathbf{n}}_{fp})dV - \frac{1}{V}\iiint(\mathbf{u}^{n}\cdot\hat{\mathbf{n}}_{fp})dV\right)\right], \tag{4}$$

where n corresponds to the n-th time step, L is the 1D component length and V is the volume of the component. The inertial term in Eq. 4 is time-averaged using a first-order scheme. Eq. 4 is only applicable to simple geometries where $\hat{\mathbf{n}}_{fp}$ and L are easily defined, and the extension of Eq. 4 to more sophisticated geometries requires further description.

For example, Grunloh and Manera (2017) extended the coupling treatment to couple CFD with an overlapping, multi-dimensional (multi-D) STH component. However, this required additional stabilization efforts that were tailored to the specific flow solver utilized by the STH code's multi-D component. Therefore it is recommended that the CFD model is only coupled with a 1D STH component. When coupling a sophisticated CFD model such as a reactor pressure vessel, the overlapping 1D STH component should be configured to ensure its coupled pressure drop correctly matches the CFD model's solution.

4. Coupling Verification and Stability

The present SAM-NekRS coupling is first verified against a canonical pump-driven closed loop. The same loop is also used to compare stability performance between the domain decomposition and domain overlapping coupling methods. Then, a canonical natural circulation loop is used to further compare stability between the methods.

4.1. Pump-driven Closed Loop

The pump-driven closed loop in Fig. 3 is implemented for the present SAM-NekRS coupling. The set pump head produces a pressure gradient in the loop, resulting in a forced flow rate and a tightly-coupled system between the pressure and velocity field. The working fluid is water at atmospheric conditions with fluid properties obtained from NIST (Linstrom and W.G. Mallard (2022)).

Table 2
Pump-driven loop verification results.

Simulation	ΔP over section [Pa]	Steady loop Re [-]
SAM standalone	6.25	25,076
Decomp. developed	6.22	25,096
Overlap. developed	6.22	25,096
Decomp. flat	7.61	24,021
Overlap. flat	7.61	24,021

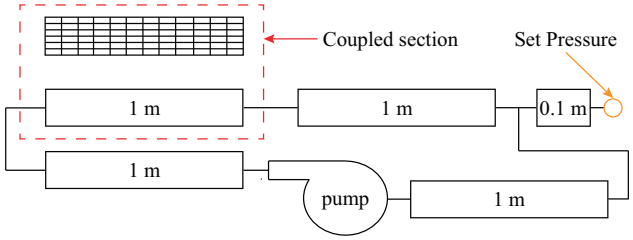

Figure 3: Pump-driven loop's setup with lengths in meters.

All straight components in Fig. 3 are round pipes with a diameter of 0.1 meters, and NekRS is used to model the coupled section of the loop. The pump head is set to 25 Pa such that the steady-state Reynolds number predicted by a SAM standalone simulation is approximately 25,000. NekRS RANS modeling is employed using the wall-resolved k-τ model (Benton et al. (1996); Shaver et al. (2020)). This model is implemented in NekRS similarly to what is described in Kok (2000).

4.1.1. Coupling Verification

To verify the coupling implementations, the simulation is ran with a SAM standalone, SAM-NekRS coupled using the domain decomposition method and SAM-NekRS coupled using the domain overlapping method. Each SAM-NekRS coupling method's simulation is ran with both a fully-developed and flat velocity profile at the inlet of the NekRS domain. Fully-developed k and τ fields are used for all NekRS simulations. For a fully-developed simulation, NekRS and SAM are expected to produce a similar pressure drop over the coupled section. However, prescribing a flat inlet velocity to NekRS produces a larger pressure drop due to flow development near the inlet of the CFD domain.

Results from each simulation are shown in Table 2. For each coupling method, using a fully-developed inlet velocity profile produces similar results in the coupled section's pressure drop and thus steady loop Reynolds number. Using a flat inlet profile produces a larger pressure drop in the NekRS domain, as expected, resulting in a lower predicted loop Reynolds number. Furthermore, each domain coupling method produces the same results for each given inlet profile, verifying both coupling methods are consistent.

4.1.2. *Stability comparison between coupling methods*

To compare the stability of domain decomposition and domain overlapping coupling methods, the change in loop velocity U_{STH} between time steps n and $n-1$ is considered relative to the steady loop velocity U_{steady}. The relative stability criteria is explicitly written in Eq. (5). Once this criteria is met, the coupled SAM-NekRS simulation is deemed numerically stable.

$$\left| \left(\frac{dU_{STH}}{dt} \right)^{n} - \left(\frac{dU_{STH}}{dt} \right)^{n-1} \right| < 1\text{e}{-3} \cdot U_{steady} \,. \quad (5)$$

To obtain a good initial guess for the loop, a coupled simulation is first preformed to obtain a "correct" steady flow rate in the loop. This steady flow rate is then used to set the initial velocity field within the NekRS domain, and the initial velocity in the SAM domain is deviated from this steady value to test the coupling's ability to return to a stable solution. For means of comparison, the total number of NekRS pressure solver iterations required to reach the stability criteria in Eq. (5) is compared while deviating the initial SAM domain's velocity. The total NekRS pressure solver iterations is used as the figure of merit because, as Fischer et al. (2021) showed, the majority of NekRS's computational effort is used for its pressure solver.

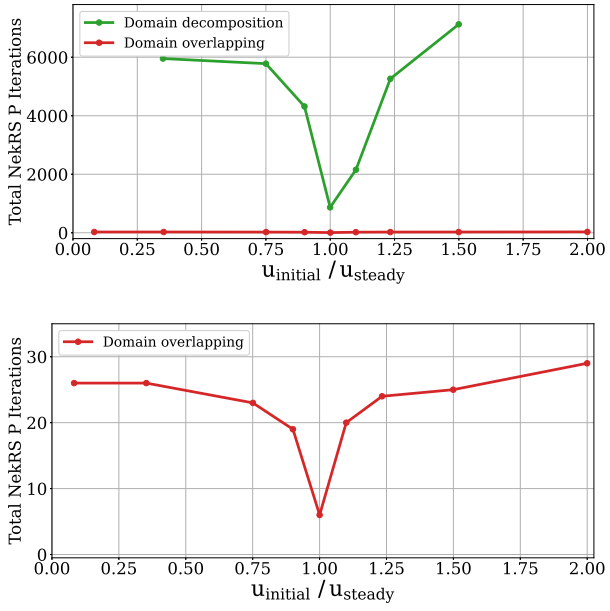

Figure 4: Pump-driven loop stability comparison between both methods (top) with a zoomed-in view (bottom).

The stability comparison between coupling methods is shown in Fig. 4, where a lower number of NekRS pressure iterations equates to a more efficient coupled simulation. In Fig. 4, the lowest number of pressure iterations is required when the initial loop velocity is the same as the steady state velocity ($u_{initial}/u_{steady} = 1$). Given the same initial velocity, the domain overlapping method requires far fewer NekRS pressure iterations to reach stability than the domain decomposition method. Also, the domain decomposition method is able to reach stability using an initial velocity 33-150% the steady velocity, whereas the domain overlapping can converge with an initial velocity 5-200% the steady velocity. Therefore, the domain overlapping method is able to handle a wider range of conditions than domain decomposition.

4.2. Natural Circulation Loop

A natural circulation loop presents a highly-coupled system where pressure losses are balanced between buoyancy (temperature) and friction (velocity) effects. The single-phase, natural circulation loop from Grunloh (2016) is used and shown in Fig. 5. For a complete description, authors refer to Grunloh (2016), but a brief description is given here. The heat q imposed and removed in Fig. 5 is set such that the steady state Reynolds number predicted is approximately 100,000 and thus sufficiently turbulent to utilize NekRS's RANS k-τ model. Water properties from NIST (Linstrom and W.G. Mallard (2022)) at a reference pressure and temperature of 15 MPa and 550 K, respectively, are used for prescribing the fluid's density, viscosity, and thermal expansion coefficient.

For the coupling setup in Fig. 5, NekRS models the bottom U-bend where 3D effects are most present. For the domain decomposition implementation, SAM models the rest of the loop not modeled by NekRS, but for the hybrid domain overlapping implementation SAM models the complete loop. The NekRS model's all-hex mesh is generated using Gmsh (Geuzaine and Remacle (2009)) while ensuring the y+ off the wall is approximately 1 due to the use of the wall-resolved RANS k-τ model. Fig. 6 shows the computational mesh utilized and the velocity field predicted by NekRS. Boundary conditions set in the NekRS model are listed in Table 3. The Inlet's velocity and RANS k-τ fields are set using a "Fully Developed" profile from a periodic pipe flow simulation. The Inlet's velocity profile is scaled such that its average velocity $\overline{U}$ matches the velocity U_{STH} coming from SAM. Furthermore, the NekRS RANS k-τ model is employed using the Boussinesq approximation in its momentum equation to account for buoyancy effects due to temperature variation. For the SAM model, to best account for friction effects in the top U-bend a U-bend form-loss coefficient from Idelchik (1986) is employed.

4.2.1. *Stability comparison between coupling methods*

To compare stability again, the change in loop velocity between time steps is considered relative to the steady loop velocity. The same relative criteria as the pump-driven loop is utilized, as written previously in Eq. (5). To obtain a good initial guess for the loop, a coupled simulation is performed to obtain a "correct" steady flow rate in the loop, which is considered the ideal initial conditions for the coupled simulation. The steady flow rate is then used to set the initial velocity field within the NekRS domain, and the initial velocity in the SAM domain is deviated from this steady

Table 3
Boundary conditions set for the U-bend's NekRS model.

Boundary	Pressure	Velocity	RANS k and τ	Temperature (T)
Inlet	-	Fully Developed with $\overline{U} = U_{STH}$	Fully Developed	Flat with T_{STH}
Outlet	0	$\nabla U = 0$	$\nabla k = \nabla \tau = 0$	$\nabla T = 0$
Wall	-	0	0	$\nabla T = 0$

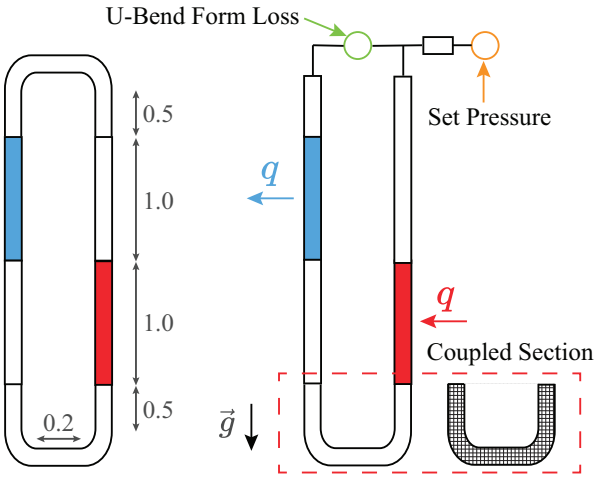

Figure 5: Natural circulation loop's setup with lengths in meters.

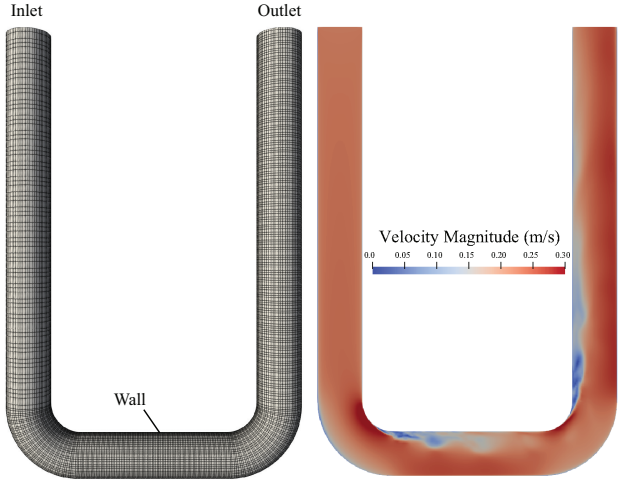

Figure 6: NekRS computational mesh with labeled boundaries (left) and NekRS RANS $k-\tau$ predicted velocity field (right).

value. The temperature field in the loop is initialized using a SAM checkpoint file.

For means of comparison, the total number of NekRS pressure solver iterations required to reach the stability criteria in Eq. (5) is compared while deviating the initial SAM domain's velocity. The results for the domain overlapping coupling are shown in Fig. 7, where the method was able to reach the stability criteria while starting with an initial velocity deviated nearly 10% from the steady velocity.

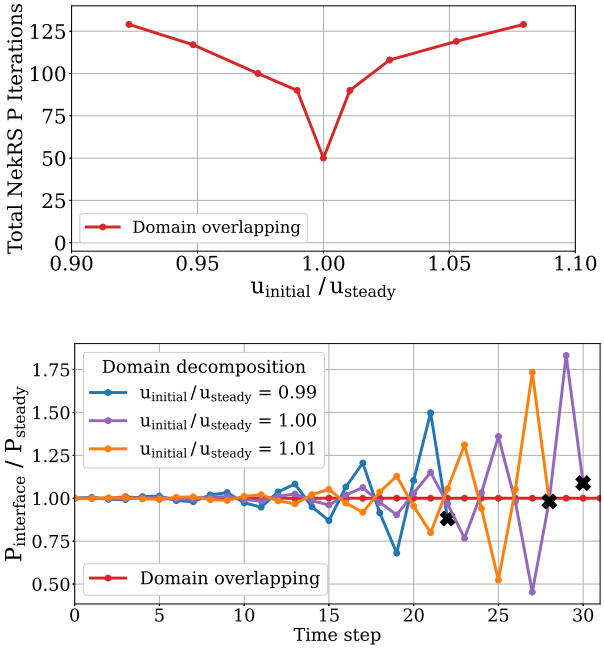

Figure 7: Natural circulation loop stability comparison between methods. Black **X**'s denote when the coupled domain decomposition simulation fails to converge.

The domain decomposition coupled simulation breaks at or before the 30th time step, which is due to the large pressure feedback effects in the loop. The normalized interface pressure at the inlet of the NekRS domain is shown in Fig. 7 for various initial flow conditions. Large pressure oscillations are seen and continue to propagate until the simulation fails to converge, whereas the domain overlapping method stays stable. This is due to the natural circulation loop's tight coupling between velocity, pressure and temperature fields, which domain decomposition with explicit coupling can not stabilize. As a whole then, Fig. 7 shows the domain overlapping method is again more stable than the domain decomposition method.

5. Coupling validation

To validate the hybrid domain overlapping coupling implementation, the double T-junction experiment from Bertolotto et al. (2009) is employed. Comparisons are made between experiment data, a SAM standalone simulation, a SAM-NekRS coupled simulation, and a TRACE-CFX coupled simulation from Bertolotto et al. (2009).

5.1. Double T-junction Setup

For a complete description of the experiment, the authors direct readers to Bertolotto et al. (2009) and Bertolotto (2011), but a brief description is given here. The double T-junction's setup is shown in Fig. 8, and it contains two loops joined by a double T-junction where one loop serves as the main line and one the recirculation line. The main line enforces a set flow rate into the double T-junction, and the recirculation line has a pump forcing flow back into the double T-junction. The system is operated at atmospheric conditions with tap water as the working fluid. A tracer (deionized water) is injected within the side loop, and its concentration is measured at three different locations using wire mesh sensors (WM). The flow rate is controlled in each loop to maintain the same Reynolds number of 23,750.

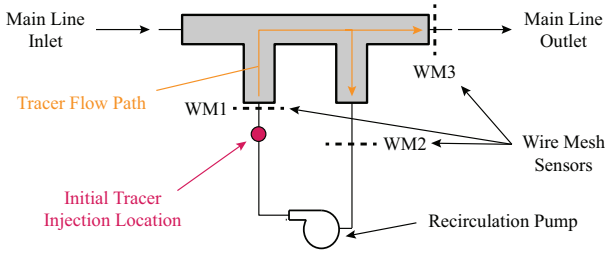

Figure 8: Schematic of the double T-junction experiment, adapted from Bertolotto et al. (2009).

5.2. NekRS Model Details

NekRS is used to model the double T-junction where 3D mixing effects are most present, and the NekRS model employs an unsteady-RANS simulation with its k-τ model along with an additional passive scalar for modeling the tracer's transport. An all-hex mesh is generated using Gmsh (Geuzaine and Remacle (2009)) while ensuring the wall y+ is approximately 1 due to the use of the wall-resolved RANS k-τ model, and Fig. 9 shows the NekRS mesh used. The NekRS predicted flow field is shown in Fig. 10 with boundaries labeled. Boundary conditions set in the NekRS model are listed in Table 4. The NekRS model's domain was extended at both outlets to ensure there's no reversed flow at these boundaries. The term "Fully Developed" in Table 4 refers to a fully-developed profile coming from a periodic simulation for the same operational Reynolds number as the experiment.

In Table 4's boundary conditions, the relative pressure at the Side outlet is set to -365 Pa such that NekRS reproduces the 1:1 flow ratio used in the experiment. In Bertolotto et al. (2009)'s CFX simulation of the same junction, the authors utilized a split-flow boundary condition for the same boundary. For the present NekRS model, setting the relative Side outlet pressure achieves the same desired result.

Both inlet boundaries in Table 4 utilize a "Fully Developed" profile from a periodic pipe flow simulation for the velocity and RANS k-τ fields. However, the Side inlet's velocity profile is scaled such that its average velocity $\overline{U}$ matches the velocity U_{STH} coming from SAM. For

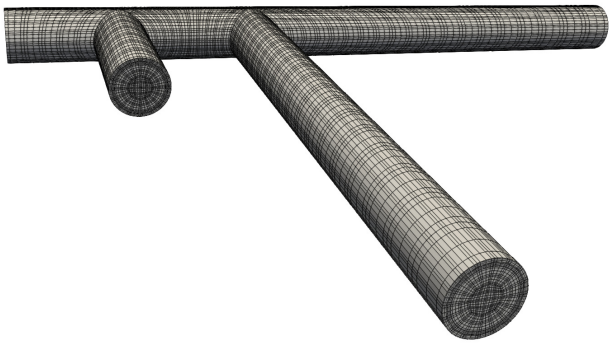

Figure 9: NekRS computational mesh used for the validation.

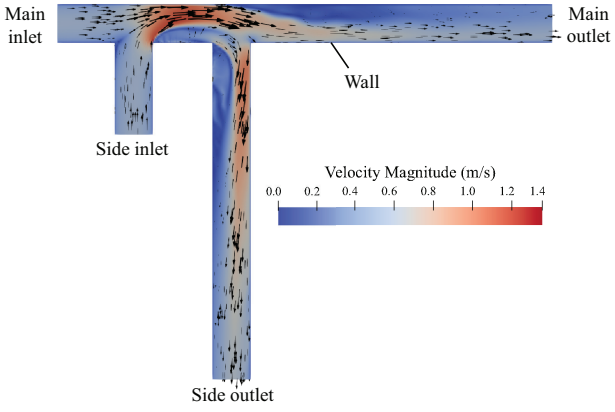

Figure 10: NekRS's predicted velocity field along the domain's centerline, with boundaries labeled.

the tracer's Side inlet boundary condition, Bertolotto et al. (2009) found that the distribution injected into the CFD domain has little influence on tracer concentrations extracted at wire mesh sensor locations. Therefore, a flat inlet distribution is used, corresponding to the value S_{STH} from SAM, where S denotes that the tracer is a passive scalar.

The initial tracer injection into the system is simulated as a prescribed, time-dependent profile following experimental wire mesh data from WM1. Doing so allows the initial tracer conditions in all of the simulations to match the initial experiment's conditions, as shown by the overlapping WM1 plot in Fig. 12. The initial injection is prescribed from within the SAM model and is transferred to the NekRS Side inlet boundary as S_{STH}. In NekRS, the tracer is modeled as a passive scalar with zero molecular diffusivity but includes turbulent diffusivity utilizing a turbulent Schmidt of 0.9, the same methodology used in Bertolotto et al. (2009).

5.3. SAM Model Details

While NekRS only models the double T-junction, SAM is used to model the entire recirculation loop, including the portion of the double T-junction that closes the recirculation loop. A schematic of the SAM standalone model is shown in

Table 4
Boundary conditions set for the double T-junction's NekRS model.

Boundary	Pressure [Pa]	Velocity	RANS k and τ	Tracer (S)
Main inlet	-	Fully Developed	Fully Developed	0
Side inlet	-	Fully Developed with $\overline{U} = U_{STH}$	Fully Developed	Flat with S_{STH}
Main outlet	0	$\nabla U = 0$	$\nabla k = \nabla \tau = 0$	$\nabla S = 0$
Side outlet	-365	$\nabla U = 0$	$\nabla k = \nabla \tau = 0$	$\nabla S = 0$
Wall	-	0	0	$\nabla S = 0$

Fig. 11. Components J1-J4 in Fig. 11 are PBBranch components while the PBTDJ and PBTDV components specify inlet flow rate and outlet reference pressure, respectively. Components M1-M3 and S1-S4 are PBOneDFluidComponents with their nodalization details shown in Table 5. To enforce the 1:1 flow ratio between the main and recirculation loop, Bertolotto et al. (2009) implemented a TRACE component to set the flow rate in the recirculation loop. In SAM, the PBPump component's "desired mass flow rate" parameter is controlled, such that a 1:1 flow ratio is maintained. The SAM model employs a passive scalar to model the tracer's transport with a diffusion coefficient of 7.6e-3 m^2/s, which acts to model any 3D mixing effects present in the recirculation loop. Bertolotto (2011) used a similar value for TRACE modeling of the same system.

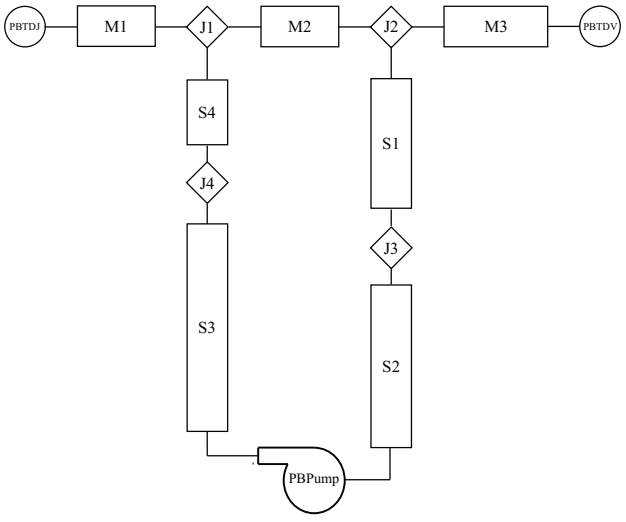

Figure 11: SAM standalone model of the double T-junction.

5.4. Coupled SAM-NekRS concentration profiles

For all present simulations, a time step size of 2.5e-4 seconds is used. The need for a small time step size is due to small elements that resulted from using Gmsh to mesh the round double T-junction for an all-hex mesh. The simulations were repeated using a NekRS polynomial order of 3, 4, and 5. Results using a polynomial order of 4 and 5 did not differ significantly, so to limit computational expenses an order of 4 is used. For all comparisons, experiment and previous TRACE-CFX coupled simulation results are compared to SAM standalone and SAM-NekRS coupled simulation results, using the present hybrid domain overlapping method.

Table 5
SAM model details for all PBOneDFluidComponents utilized.

Label	Length (meters)	No. of elements
M1	0.12	4
M2	0.12	24
M3	0.16	32
S1	0.20	40
S2	2.51	502
S3	2.79	559
S4	0.10	20

The cross-section averaged concentration over time for the first flow through of tracer is shown in Fig. 12. These plots serve to validate the NekRS model in the coupled SAM-NekRS simulation because during the first flow through, the coupled SAM-NekRS simulation transports tracer only within its NekRS domain. WM1's concentration profile in all simulations matches the experiment exactly because this is the initial tracer injection used for all simulations. SAM-NekRS coupled results for WM2 and WM3 match the experiment better than the SAM standalone simulation while producing similar results to previous TRACE-CFX coupling. The SAM standalone simulation under predicts tracer recirculating in the recirculation loop through WM2 and over predicts tracer leaving the system through WM3. This is due to the 3D mixing effects present within the double T-junction, which SAM doesn't take into account when using its 1D components. Explicitly, due to equal mass flow rates in the main line and recirculation line, SAM splits the tracer within the double T-junction equally such that half of the tracer leaves the system through WM3 and half is recirculated through WM2. In the experiment however, the tracer concentration does not split according to the mass flow rate and instead has a tendency to deviate into the side loop.

After the first flow through, the tracer either leaves the system through WM3 or is recirculated through the recirculation loop and re-enters the double T-Junction at WM1. As tracer leaves the system, less and less tracer is recirculated through the wire mesh sensors. This is shown by the decreasing magnitude of tracer concentration in Fig. 12 and Fig. 13 over time.

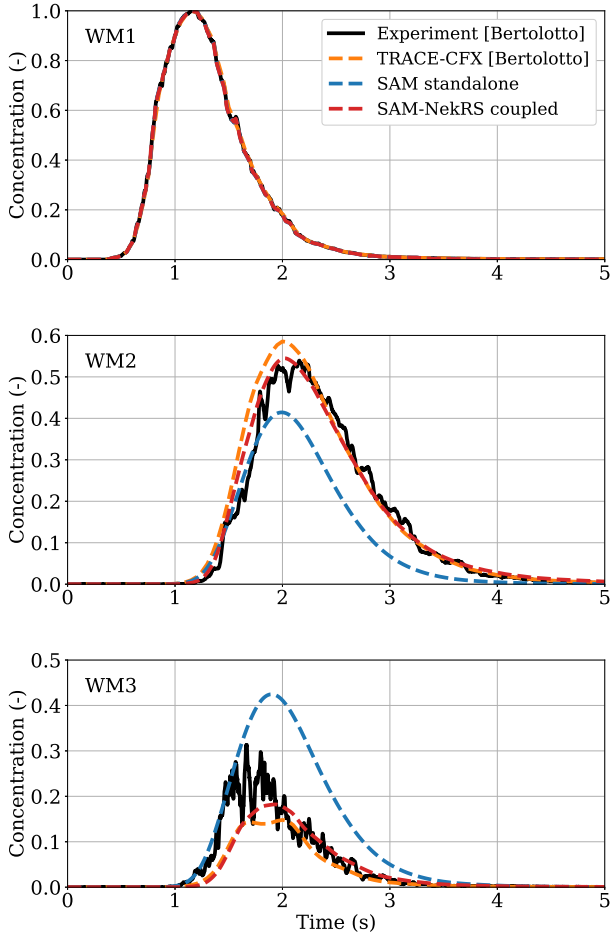

Figure 12: Cross-section averaged tracer concentration plots for the first tracer flow through.

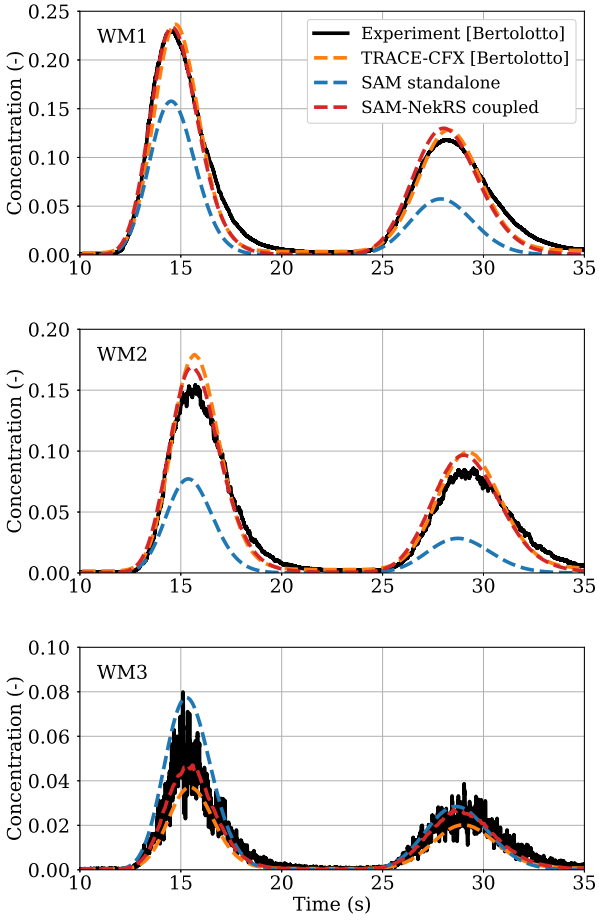

Figure 13: Cross-section averaged tracer concentration plots for the second and third tracer flow throughs.

The second and third tracer flow throughs are shown in Fig. 13. These plots serve to validate the complete SAM-NekRS coupled model because now the tracer is transported by both the SAM domain and NekRS domain. The SAM standalone simulation continues to under predict tracer recirculation through WM2 and over predict tracer leaving the system through WM3. SAM-NekRS coupled results are similar to previous TRACE-CFX results, but for WM2 and WM3, the present SAM-NekRS results match more closely with the experiment. This is likely due to a combination of effects stemming from differences in the codes and models used between the SAM-NekRS and TRACE-CFX coupling. SAM utilizes higher-order numerical methods than TRACE, resulting in a low amount of numerical diffusion that would greatly affect passive scalar transport, both spatially and temporally. As for the CFD models, NekRS uses the RANS k-τ model whereas CFX used the RANS SST (Shear Stress Transport) model. Different RANS models are expected to predict different flow fields, so for the double T-junction the NekRS RANS k-τ model likely predicts a flow field more similar to the experiment compared to the CFX RANS SST model.

5.5. Coupled SAM-NekRS concentration integrals

Next, concentration integrals are used to compare the total concentration of tracer passing through each wire mesh sensor over time. The concentration integrals are shown in Fig. 14, where each integral increases three times, one for each flow through of tracer. In Fig. 14 it is even more apparent that the SAM standalone simulation under predicts tracer recirculation (through WM2) and over predicts tracer leaving the system (through WM3). Furthermore, SAM-NekRS coupled results match experiment more closely than the previous TRACE-CFX coupling, with the largest difference being in the WM3 concentration integral plot. This is likely due to differences in the predicted velocity field between NekRS's RANS k-τ model and CFX's RANS SST model used by Bertolotto et al. (2009).

Although it may be of interest to compare 2D contour plots of the tracer concentration between the SAM-NekRS coupled simulation and the experiment, 2D wire mesh sensor data was not published by Bertolotto et al. (2009). Furthermore, the goal of a coupled STH-CFD model is to provide more-accurate results compared to an STH standalone model, but such 2D contour data does not exist in the STH standalone model. Therefore, only cross-section

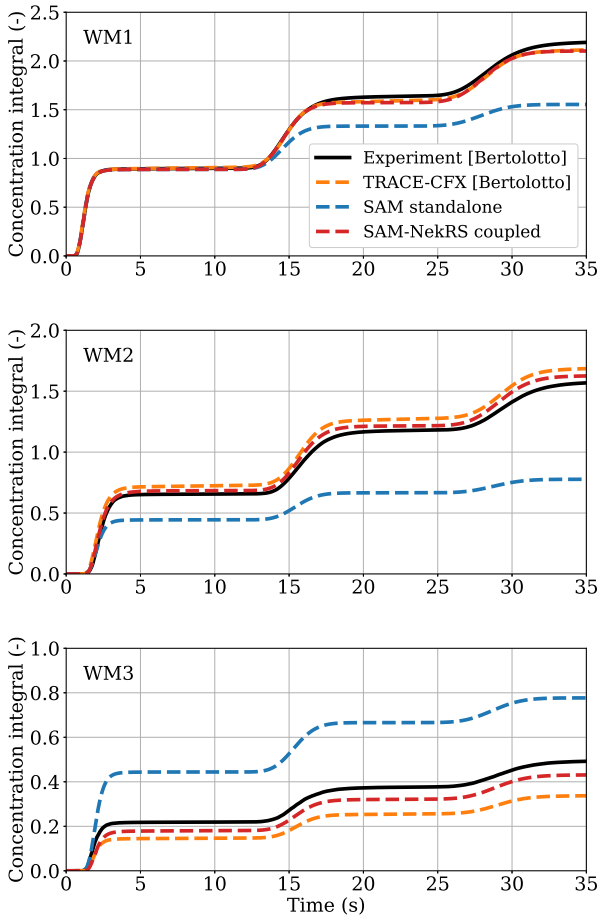

Figure 14: Concentration integrals through each wire mesh sensor location.

averaged concentration plots and concentration integral plots were compared between the simulations and experiment.

6. Conclusions and Future Work

The coupling between the STH code SAM and the CFD code NekRS has been presented using domain decomposition and hybrid domain overlapping coupling methods with an explicit coupling scheme. The numerical stability of each coupling method was compared using a pump-driven closed loop and natural circulation loop, both of which contain tightly-coupled loop configurations. In both cases, domain overlapping was shown to be more stable, especially in the natural circulation loop case where the domain decomposition method's simulation diverged.

The proposed hybrid domain overlapping coupling method was validated against a double T-junction experiment from open literature. The present SAM-NekRS coupled simulation was able capture the complexity of 3D mixing in the double T-junction. Furthermore, the SAM-NekRS coupling provided superior results matching experiment data better than previous TRACE-CFX coupling of the same system. This is partly due to SAM utilizing higher-order numerical methods than TRACE, resulting in low amount of numerical diffusion that would greatly affect passive scalar transport. Also, the NekRS model utilizes a different RANS model than the CFX model, so the NekRS RANS k-τ model likely predicts a flow field more similar to the experiment as compared to the CFX RANS SST model.

With the coupling method validated on a small system with passive scalar coupling, the method requires further validation against experimental data of large systems containing mass, momentum and energy coupling. One promising facility is the Tall-3D STH/CFD benchmark facility from Grishchenko et al. (2015). TALL-3D is a Lead-Bismuth Eutectic (LBE) loop built for validating STH/CFD coupling efforts for advanced nuclear reactor systems. The facility's benchmark contains a transient from forced-circulation to natural circulation, emulating a protected loss of flow accident scenario in a pool-type, liquid metal cooled fast reactor. Therefore, validating the present coupling against this facility is of great interest.

Declaration of Competing Interest

The authors declare that they have no known competing financial interests or personal relationships that could have appeared to influence the work reported in this paper.

Acknowledgments

This work was funded through a National Science Foundation Graduate Research Fellowship under Grant No. DGE 1256260; the U.S. Department of Energy Office of Nuclear Energy under contract DE-AC02-06CH11357; and the U.S. Department of Energy Office of Nuclear Energy's Nuclear Energy University Program under contract DE-NE0008984. Any opinion, findings, and conclusions or recommendations expressed in this material are those of the authors and do not necessarily reflect the views of the National Science Foundation.

References

A. J. Huning, S. Chandrasekaran, S. Garimella, A review of recent advances in htgr cfd and thermal fluid analysis, Nuclear Engineering and Design 373 (2021) 111013.

Z. Wu, C. Lu, S. Morgan, S. Bilbao y Leon, M. Bucknor, A status review on the thermal stratification modeling methods for sodium-cooled fast reactors, Progress in Nuclear Energy 125 (2020) 103369.

B. Smith, U. Bieder, E. Graffard, M. Heitsch, M. Henriksson, T. Höhne, E. Komen, J. Mahaffy, F. Moretti, T. Morii, P. Mühlbauer, U. Rohde, M. Scheuerer, C.-H. Song, G. Zigh, Assessment of Computational Fluid Dynamics (CFD) for Nuclear Reactor Safety Problems, Technical Report NEA/CSNI/R(2007)13, OECD Nuclear Energy Agency, 2008. doi:10.2172/1762134.

J. Long, B. Zhang, B.-W. Yang, S. Wang, Review of researches on coupled system and cfd codes, Nuclear Engineering and Technology 53 (2021) 2775–2787.

A. Pucciarelli, A. Toti, D. Castelliti, F. Belloni, K. Van Tichelen, M. Moscardini, F. Galleni, N. Forgione, Coupled system thermal hydraulics/cfd models: General guidelines and applications to heavy liquid metals, Annals of Nuclear Energy 153 (2021) 107990.

D. Aumiller, E. Tomlinson, R. Bauer, A coupled relap5-3d/cfd methodology with a proof-of-principle calculation, Nuclear Encardinal2021NT gineering and Design 205 (2001) 83–90.

R. R. Schultz, W. L. Weaver, Using the relap5-3d advanced systems analysis code with commercial and advanced cfd software, in: Proceedings of the International Conference on Nuclear Engineering. Book of abstracts : ICONE11-36545, volume 2003, 2003, p. 323. doi:10.1299/jsmeicone.2003.323.

N. A. Anderson, Coupling RELAP5-3D and Fluent to analyze a Very High Temperature Reactor (VHTR) outlet plenum, Ph.D. thesis, Texas A&M University, 2006.

A. Papukchiev, G. Lerchl, C. Waata, T. Frank, Extension of the simulation capabilities of the 1d system code athlet by coupling with the 3d cfd software package ansys cfx, in: Proceedings NURETH-13, 2009.

Y. Liu, H. ZHANG, B.-s. JIA, Research on coupling between relap5 and cfx codes, Atomic Energy Science and Technology 44 (2010) 304.

Y. Yan, et al., Coupled cfd-system-code simulation of a gas cooled reactor, in: International Conference on Mathematics and Computational Methods Applied to Nuclear Science and Engineering (M&C 2011), 2011.

R. Bavière, N. Tauveron, F. Perdu, E. Garré, S. Li, A first system/cfd coupled simulation of a complete nuclear reactor transient using cathare2 and trio-u. preliminary validation on the phénix reactor natural circulation test, Nuclear Engineering and Design 277 (2014) 124–137.

H. K. Cho, Y. J. Cho, H. Y. Yoon, Heat structure coupling of cupid and mars for the multi-scale simulation of the passive auxiliary feedwater system, Nuclear Engineering and Design 273 (2014) 459–468.

W. Li, X. Wu, D. Zhang, G. Su, W. Tian, S. Qiu, Preliminary study of coupling cfd code fluent and system code relap5, Annals of Nuclear Energy 73 (2014) 96–107.

D. Martelli, N. Forgione, G. Barone, A. Del Nevo, I. Di Piazza, M. Tarantino, Coupled simulations of natural and forced circulation tests in nacie facility using relap5 and ansys fluent codes, in: International Conference on Nuclear Engineering, volume 45943, American Society of Mechanical Engineers, 2014, p. V004T10A020.

T. Watanabe, Y. Anoda, M. Takano, System–cfd coupled simulations of flow instability in steam generator u tubes, Annals of Nuclear Energy 70 (2014) 141–146.

F. Tangtao, T. Wenxi, S. Ping, Z. Dalin, S. Guanghui, Q. Suizheng, Transient characteristics analysis of water hammer phenomena based on coupling program, Atomic Energy Science and Technology 51(8) (2017) 1364–1370.

D. Bertolotto, A. Manera, S. Frey, H.-M. Prasser, R. Chawla, Single-phase mixing studies by means of a directly coupled cfd/system-code tool, Annals of Nuclear Energy 36 (2009) 310–316. PHYSOR 2008.

G. Theodoridis, A. Papukchiev, D. Scholz, G. Lerchl, A New Data-Driven ATHLET – ANSYS CFD Coupling Method for Efficient Simulation of Nuclear Power Plant Circuits, in: International Conference on Nuclear Engineering, 2014. URL: https://doi.org/10.1115/ICONE22-31119. doi:10.1115/ICONE22-31119, v004T10A047.

A. Toti, J. Vierendeels, F. Belloni, Improved numerical algorithm and experimental validation of a system thermal-hydraulic/cfd coupling method for multi-scale transient simulations of pool-type reactors, Annals of Nuclear Energy 103 (2017) 36–48.

I. Park, J. Lee, S. Lee, H. Yoon, J. Jeong, An implicit code coupling of 1-d system code and 3-d in-house cfd code for multi-scaled simulations of nuclear reactor transients, Annals of Nuclear Energy 59 (2013) 80–91.

T. Grunloh, A. Manera, A novel domain overlapping strategy for the multiscale coupling of cfd with 1d system codes with applications to transient flows, Annals of Nuclear Energy 90 (2016) 422–432.

R. Hu, et al., SAM Theory Manual, Technical Report ANL/NSE-17/4 Rev. 1, Argonne National Laboratory, 2021.

P. Fischer, S. Kerkemeier, M. Min, Y. Lan, M. Phillips, T. Rathnayake, E. Merzari, A. Tomboulides, A. Karakus, N. Chalmers, T. Warburton, NekRS, a GPU-Accelerated Spectral Element Navier-Stokes Solver, 2021. URL: https://arxiv.org/abs/2104.05829, arXiv:2104.05829.

E. Merzari, H. Yuan, M. Min, D. Shaver, R. Rahaman, P. Shriwise, P. Romano, A. Talamo, Y. Lan, D. Gaston, R. Martineau, P. Fischer, Y. Hassan, Cardinal: A lower length-scale multiphysics simulator for pebble-bed reactors, Nuclear Technology (2021).

A. Novak, D. Andrs, P. Shriwise, J. Fang, H. Yuan, D. Shaver, E. Merzari, P. Romano, R. Martineau, Coupled monte carlo and thermal-fluid modeling of high temperature gas reactors using cardinal, Annals of Nuclear Energy 177 (2022) 109310.

C. J. Permann, D. R. Gaston, D. Andrš, R. W. Carlsen, F. Kong, A. D. Lindsay, J. M. Miller, J. W. Peterson, A. E. Slaughter, R. H. Stogner, R. C. Martineau, MOOSE: Enabling massively parallel multiphysics simulation, SoftwareX 11 (2020) 100430.

B. S. Kirk, J. W. Peterson, R. H. Stogner, G. F. Carey, libMesh: A C++ Library for Parallel Adaptive Mesh Refinement/Coarsening Simulations, Engineering with Computers 22 (2006) 237–254. https://doi.org/10.1007/s00366-006-0049-3.

S. Balay, S. Abhyankar, M. F. Adams, S. Benson, J. Brown, P. Brune, K. Buschelman, E. M. Constantinescu, L. Dalcin, A. Dener, V. Eijkhout, W. D. Gropp, V. Hapla, T. Isaac, P. Jolivet, D. Karpeev, D. Kaushik, M. G. Knepley, F. Kong, S. Kruger, D. A. May, L. C. McInnes, R. T. Mills, L. Mitchell, T. Munson, J. E. Roman, K. Rupp, P. Sanan, J. Sarich, B. F. Smith, S. Zampini, H. Zhang, H. Zhang, J. Zhang, PETSc Web page, https://petsc.org/, 2022. URL: https://petsc.org/.

N. Chalmers, A. Karakus, A. P. Austin, K. Swirydowicz, T. Warburton, libParanumal: a performance portable high-order finite element library, 2022. URL: https://github.com/paranumal/libparanumal. doi:10.5281/zenodo.4004744, release 0.5.0.

P. Fischer, E. Merzari, M. Min, S. Kerkemeier, Y.-H. Lan, M. Phillips, T. Rathnayake, A. Novak, D. Gaston, N. Chalmers, T. Warburton, Highly optimized full-core reactor simulations on summit, 2021. URL: https://arxiv.org/abs/2110.01716. doi:10.48550/ARXIV.2110.01716.

E. Merzari, J. Fang, D. R. Shaver, Y.-H. Lan, M. Min, P. F. Fischer, R. O. Rahaman, P. K. Romano, Initial full core SMR simulations with NekRS, Technical Report, Argonne National Laboratory, 2020. URL: https://www.osti.gov/biblio/1762135. doi:10.2172/1762135.

D. R. Gaston, C. J. Permann, J. W. Peterson, A. E. Slaughter, D. Andrš, Y. Wang, M. P. Short, D. M. Perez, M. R. Tonks, J. Ortensi, L. Zou, R. C. Martineau, Physics-based multiscale coupling for full core nuclear reactor simulation, Annals of Nuclear Energy 84 (2015) 45–54.

A. Novak, D. Shaver, B. Feng, Conjugate heat transfer coupling of nekrs and moose for bypass flow modeling, in: Proceedings ANS, 2021.

A. Novak, D. Andrs, P. Shriwise, D. Shaver, P. Romano, E. Merzari, P. Keutelian, Coupled monte carlo and thermal-hydraulics modeling of a prismatic gas reactor fuel assembly using cardinal, in: Proceedings PHYSOR, 2022a.

A. Novak, P. Shriwise, R. Rahaman, P. Romano, E. Merzari, D. Gaston, Coupled monte carlo transport and conjugate heat transfer for wire-wrapped bundles within the moose framework, in: Proceedings NURETH, 2022b.

A. Huxford, V. Coppo Leite, E. Merzari, L. Zou, V. Petrov, A. Manera, Development of innovative overlapping-domain coupling between sam and nekrs, in: Proceedings NURETH, 2022.

T. Grunloh, A. Manera, A novel multi-scale domain overlapping cfd/sth coupling methodology for multi-dimensional flows relevant to nuclear applications, Nuclear Engineering and Design 318 (2017) 85–108.

P. Linstrom, E. W.G. Mallard, NIST Chemistry WebBook, Technical Report NIST Standard Reference Database Number 69, National Institute of Standards and Technology, Gaithersburg, MD, 2022. doi:10.18434/T4D303.

J. Benton, G. Kalitzin, A. Gould, Application of two-equation turbulence models in aircraft design, AIAA 34th Aerospace Sciences Meeting and Exhibit, 1996. URL: https://arc.aiaa.org/doi/abs/10.2514/6.1996-327. doi:10.2514/6.1996-327. arXiv:https://arc.aiaa.org/doi/pdf/10.2514/6.1996-327.

D. Shaver, A. Obabko, A. Tomboulides, V. C. Leite, Y.-H. Lan, M. Min, P. F. Fischer, C. Boyd, Nek5000 developments in support of industry and the NRC, Technical Report ANL/NSE-20/48, Argonne National Laboratory, 2020. doi:10.2172/1762134.

S. Kok, J.C.; Spekreijse, Efficient and accurate implementation of the k-omega turbulence model in the NLR multi-block Navier-Stokes system,

Technical Report NLR NLR-TP-2000-144, National Aerospace Laboratory, 2000.

P. Fischer, E. Merzari, M. Min, S. Kerkemeier, Y.-H. Lan, M. Phillips, T. Rathnayake, A. Novak, D. Gaston, N. Chalmers, T. Warburton, Highly optimized full-core reactor simulations on summit, 2021. URL: https://arxiv.org/abs/2110.01716. doi:10.48550/ARXIV.2110.01716.

T. Grunloh, A Novel Multi-Scale Domain Overlapping CFD/STH Coupling Methodology for Multi-Dimensional Flows Relevant to Nuclear Applications, Ph.D. thesis, University of Michigan, 2016.

C. Geuzaine, J.-F. Remacle, Gmsh: A 3-D finite element mesh generator with built-in pre- and post-processing facilities, International Journal for Numerical Methods in Engineering 79 (2009) 1309–1331.

I. E. Idelchik, Handbook of hydraulic resistance (2nd revised and enlarged edition), 1986.

D. Bertolotto, Coupling a System Code with Computational Fluid Dynamics for the Simulation of Complex Coolant Reactivity Effects, Ph.D. thesis, École Polytechnique Fédérale de Lausanne, 2011.

D. Grishchenko, M. Jeltsov, K. Kööp, A. Karbojian, W. Villanueva, P. Kudinov, The tall-3d facility design and commissioning tests for validation of coupled sth and cfd codes, Nuclear Engineering and Design 290 (2015) 144–153. Thermal-Hydraulics of Innovative Nuclear Systems.